Hindawi
Advances in High Energy Physics
Volume 2018, Article ID 7682325, 9 pages
https://doi.org/10.1155/2018/7682325

Research Article

A Description of the Transverse Momentum Distributions of Charged Particles Produced in Heavy Ion Collisions at RHIC and LHC Energies

Jia-Qi Hui, Zhi-Jin Jiang, and Dong-Fang Xu

College of Science, University of Shanghai for Science and Technology, Shanghai 200093, China

Correspondence should be addressed to Zhi-Jin Jiang; jzj265@163.com

Received 5 November 2017; Revised 27 January 2018; Accepted 6 March 2018; Published 8 April 2018

Academic Editor: Bhartendu K. Singh

By assuming the existence of memory effects and long-range interactions, nonextensive statistics together with relativistic hydrodynamics including phase transition are used to discuss the transverse momentum distributions of charged particles produced in heavy ion collisions. It is shown that the combined contributions from nonextensive statistics and hydrodynamics can give a good description of the experimental data in Au+Au collisions at $\sqrt{s_{NN}} = 200$ GeV and in Pb+Pb collisions at $\sqrt{s_{NN}} = 2.76$ TeV for $\pi^{\pm}$ and $K^{\pm}$ in the whole measured transverse momentum region and for $p(\overline{p})$ in the region of $p_T \leq 2.0$ GeV/c. This is different from our previous work using the conventional statistics plus hydrodynamics, where the describable region is only limited in $p_T \leq 1.1$ GeV/c.

1. Introduction

The primary goals of the experimental programs performed in high energy heavy ion collisions are to find the deconfined nuclear matter, namely, the quark-gluon plasma (QGP), which is believed to have filled in the early universe several microseconds after the Big Bang. Therefore, studying the properties of QGP is important for both particle physics and cosmology. In the past decade, a number of bulk observables about charged particles, such as the Fourier coefficients v_n of azimuth-angle distributions [1, 2], transverse momentum spectra [3–8], and pseudorapidity distributions [9–12], have been extensively studied in nuclear collisions at both RHIC and LHC energies. These investigations have shown that the matter created in these collisions is in the state of strongly coupled quark-gluon plasma (sQGP), exhibiting a clear collective behavior nearly like a perfect fluid with very low viscosity [13–31]. Therefore, the space-time evolution of sQGP can be described in the scope of relativistic hydrodynamics, which connects the static aspects of sQGP properties and the dynamical aspects of heavy ion collisions [32].

In our previous work [33], by considering the effects of thermalization, we once used a hydrodynamic model incorporating phase transition in analyzing the transverse momentum distributions of identified charged particles produced in heavy ion collisions. In that model, the quanta of hot and dense matter are supposed to obey the standard statistical distributions and the experimental measurements in Au+Au collisions at $\sqrt{s_{NN}} = 200$ and 130 GeV can be well matched up in the region of $p_T \leq 1.1$ GeV/c. Known from the investigations in [34, 35], the memory effects and long-range interactions might appear in the hot and dense matter. This guarantees the reasonableness of nonextensive statistics in describing the thermal motions of quanta of hot and dense matter, since this new statistics is just suitable for the thermodynamic system including memory effects and long-range interactions. Hence, in this paper, on the basis of hydrodynamics taking phase transition into consideration, we will use nonextensive statistics instead of conventional statistics to simulate the transverse collective flow of the matter created in collisions.

The nonextensive statistics are also known as Tsallis nonextensive thermostatistics, which were first proposed by Tsallis in 1988 in his pioneering work [36]. This statistical theory overcomes the shortcomings of the conventional statistics in many physical problems with long-range interactions, memory effects, or fractal space-time constrains [34]. It has a wide range of applications in high energy physics [37–39], astrophysical self-gravitating systems [40], cosmology [41], the solar neutrino problem [42], many-body theory, dynamical linear response theory, and variational methods [43].

In Section 2, a brief description is given on the employed hydrodynamics, presenting its analytical solutions. The solutions are then used in Section 3 to formulate the transverse momentum distributions of charged particles produced in heavy ion collisions in the light of nonextensive statistics and Cooper-Frye prescription. The last section is about conclusions.

2. A Brief Introduction to the Hydrodynamic Model

The key points of the hydrodynamic model [18] used in the present paper are as follows.

The expansions of fluid follow the continuity equation

$$\frac{\partial T^{\mu\nu}}{\partial x^{\nu}} = 0, \quad \mu, \nu = 0, 1, \tag{1}$$

where $x^{\nu} = (x^0, x^1) = (t, z)$ and

$$T^{\mu\nu} = (\varepsilon + p)\, u^{\mu} u^{\nu} - p g^{\mu\nu} \tag{2}$$

is the energy-momentum tensor of perfect fluid, where $g^{\mu\nu} = \mathrm{diag}(1, -1)$ is the metric tensor and $u^{\mu} = (u^0, u^1) = (\cosh y_F, \sinh y_F)$ is the four-velocity of fluid with rapidity y_F. The energy density ε and the pressure p of fluid are related by the sound speed c_s via the equation of state

$$\frac{dp}{d\varepsilon} = \frac{s dT}{T ds} = c_s^2, \tag{3}$$

where T is the temperature and s is the entropy density of fluid.

Projecting (1) to the direction of u_{μ} gives

$$\frac{\partial (s u^{\nu})}{\partial x^{\nu}} = 0, \tag{4}$$

which is the continuity equation for entropy conservation. Projecting (1) to the direction Lorentz perpendicular to u_{μ} leads to the following equation:

$$\frac{\partial (T \sinh y_F)}{\partial t} + \frac{\partial (T \cosh y_F)}{\partial z} = 0, \tag{5}$$

which means the existence of scalar function ϕ satisfying

$$\begin{aligned} \frac{\partial \phi}{\partial t} &= T \cosh y_F, \\ \frac{\partial \phi}{\partial z} &= -T \sinh y_F. \end{aligned} \tag{6}$$

From ϕ and Legendre transformation, Khalatnikov potential χ is introduced by

$$\chi = \phi - tT \cosh y_F + zT \sinh y_F, \tag{7}$$

which makes the coordinates of (t, z) transform to

$$\begin{aligned} t &= \frac{e^{\omega}}{T_0} \left(\frac{\partial \chi}{\partial \omega} \cosh y_F + \frac{\partial \chi}{\partial y_F} \sinh y_F \right), \\ z &= \frac{e^{\omega}}{T_0} \left(\frac{\partial \chi}{\partial \omega} \sinh y_F + \frac{\partial \chi}{\partial y_F} \cosh y_F \right), \end{aligned} \tag{8}$$

where T_0 is the initial temperature of fluid and $\omega = \ln(T_0/T)$. In terms of χ, (4) can be rewritten as the so-called telegraphy equation:

$$\frac{\partial^2 \chi}{\partial \omega^2} - 2\beta \frac{\partial \chi}{\partial \omega} - \frac{1}{c_s^2} \frac{\partial^2 \chi}{\partial y_F^2} = 0, \quad \beta = \frac{1 - c_s^2}{2c_s^2}. \tag{9}$$

With the expansions of created matter, its temperature becomes lower and lower. When the temperature reduces from initial temperature T_0 to the critical temperature T_c, the matter transforms from the sQGP state to the hadronic state. The produced hadrons are initially in the violent and frequent collisions, which are mainly inelastic. Hence, the abundance of identified hadrons is constantly changing. Furthermore, the mean free paths of these primary hadrons are very short. In sQGP, $c_s = c_0 = 1/\sqrt{3}$. The evolution of them still satisfies (9) with only difference being the values of c_s. In the hadronic state, $0 < c_s = c_h \leq c_0$. At the point of phase transition, c_s is discontinuous.

The solutions of (9) for the sQGP and hadronic state are, respectively [18],

$$\chi_0(\omega, y_F) = \frac{Q_0 c_0}{2} e^{\beta_0 \omega} I_0 \left(\beta_0 \sqrt{\omega^2 - c_0^2 y_F^2} \right), \tag{10}$$

$$\begin{aligned} &\chi_h(\omega, y_F) \\ &\quad = \frac{Q_0 c_0}{2} e^{\beta_h (\omega - \omega_c) + \beta_0 \omega_c} I_0 \left(\beta_h c_h \sqrt{y_h^2(\omega) - y_F^2} \right), \end{aligned} \tag{11}$$

where Q_0 is a constant determined by fitting the theoretical results with experimental data, I_0 is the 0th-order modified Bessel function, and

$$\begin{aligned} \beta_0 &= \frac{\left(1 - c_0^2\right)}{2c_0^2} = 1, \\ \beta_h &= \frac{\left(1 - c_h^2\right)}{2c_h^2}, \\ \omega_c &= \ln\left(\frac{T_0}{T_c}\right), \\ y_h(\omega) &= \left[\frac{(\omega - \omega_c)}{c_h} \right] + \left(\frac{\omega_c}{c_0} \right). \end{aligned} \tag{12}$$

3. The Transverse Momentum Distributions of Charged Particles Produced in Heavy Ion Collisions

3.1. The Energy of Quantum of Produced Matter. In the nonextensive statistics, there are two basic postulations [36, 40].

(a) The entropy of a statistical system possesses the form of

$$s_q = \frac{1}{q-1}\sum_{i=1}^{\Omega} p_i\left(1 - p_i^{q-1}\right), \tag{13}$$

where p_i is the probability of a given microstate among Ω different ones and q is a real parameter.

(b) The mean value of an observable O is given by

$$\overline{O}_q = \sum_{i=1}^{\Omega} p_i^q O_i, \tag{14}$$

where O_i is the value of an observable O in the microstate i.

From the above two postulations, the average occupational number of the quantum in the state with temperature T can be written in a simple analytical form [44]:

$$\overline{n}_q = \frac{1}{\left[1 + (q-1)(E-\mu_B)/T\right]^{1/(q-1)} + \delta}, \tag{15}$$

where E is the energy of quantum and μ_B is its baryochemical potential. $\delta = 1$ for fermions, and $\delta = -1$ for bosons. In the limit of $q \to 1$, it reduces to the conventional Fermi-Dirac or Bose-Einstein distributions. Hence, the value of q reflects the discrepancies of nonextensive statistics from the conventional ones. Known from (15), the average energy of quantum in the state with temperature T reads

$$\overline{E}_q = \frac{m_T \cosh(y - y_F)}{\left[1 + (q-1)(m_T \cosh(y - y_F) - \mu_B)/T\right]^{1/(q-1)} + \delta}, \tag{16}$$

where y is the rapidity of quantum and $m_T = \sqrt{p_T^2 + m^2}$ is its transverse mass with rest mass m and transverse momentum p_T.

3.2. The Rapidity Distributions of Charged Particles in the State of Fluid. In terms of Khalatnikov potential χ, the rapidity distributions of charged particles in the state of fluid can be written as [45]

$$\frac{dN}{dy_F} = \frac{Q_0 c_0}{2} A(b)\left(\cosh y \frac{dz}{dy_F} - \sinh y \frac{dt}{dy_F}\right), \tag{17}$$

where

$$A(b) = 2r^2 \arccos\frac{b}{2r} - b\sqrt{r^2 - \left(\frac{b}{2}\right)^2} \tag{18}$$

is the area of overlap region of collisions, b is impact parameter, and r is the radius of colliding nucleus. From (8), the expression in the round brackets in (17) becomes

$$\begin{aligned}\cosh y \frac{dz}{dy_F} - \sinh y \frac{dt}{dy_F} &= \frac{1}{T} c_s^2 \frac{\partial}{\partial \omega}\left(\chi + \frac{\partial \chi}{\partial \omega}\right)\cosh(y - y_F) \\ &\quad - \frac{1}{T}\frac{\partial}{\partial y_F}\left(\chi + \frac{\partial \chi}{\partial \omega}\right)\sinh(y - y_F).\end{aligned} \tag{19}$$

3.3. The Transverse Momentum Distributions of Charged Particles Produced in Heavy Ion Collisions. Along with the expansions of hadronic matter, its temperature becomes even lower. As the temperature drops to kinetic freeze-out temperature T_f, the inelastic collisions among hadronic matter stop. The yields of identified hadrons remain unchanged, becoming the measured results. According to Cooper-Frye scheme [45], the invariant multiplicity distributions of charged particles take the form [18, 45, 46]

$$\frac{d^2N}{2\pi p_T dy dp_T} = \frac{1}{(2\pi)^3}\int_{-y_h(\omega_f)}^{y_h(\omega_f)}\left(\frac{dN}{dy_F}\overline{E}_q\right)\Big|_{T=T_f} dy_F, \tag{20}$$

where $\omega_f = \ln(T_0/T_f)$ and the integrand takes values at the moment of $T = T_f$.

Substituting χ in (19) by χ_h of (11), it becomes

$$\begin{aligned}\left(\cosh y \frac{dz}{dy_F} - \sinh y \frac{dt}{dy_F}\right)\Big|_{T=T_f} &= \frac{1}{T_f}(\beta_h c_h)^2 \\ &\cdot e^{\beta_h(\omega-\omega_c)+\beta_0\omega_c}\left[B(\omega_f, y_F)\sinh(y - y_F)\right. \\ &\left. + C(\omega_f, y_F)\cosh(y - y_F)\right],\end{aligned} \tag{21}$$

where

$$\begin{aligned}B(\omega_f, y_F) &= \frac{\beta_h y_F}{\lambda(\omega_f, y_F)}\left\{\frac{\beta_h c_h y_h(\omega_f)}{\lambda(\omega_f, y_F)} I_0\left[\lambda(\omega_f, y_F)\right]\right. \\ &\left. + \left[\frac{\beta_h + 1}{\beta_h} - \frac{2\beta_h c_h y_h(\omega_f)}{\lambda^2(\omega_f, y_F)}\right] I_1\left[\lambda(\omega_f, y_F)\right]\right\}, \\ C(\omega_f, y_F) &= \left\{\frac{\beta_h + 1}{\beta_h} + \frac{\left[\beta_h c_h y_h(\omega_f)\right]^2}{\lambda^2(\omega_f, y_F)}\right\} \\ &\cdot I_0\left[\lambda(\omega_f, y_F)\right] + \frac{1}{\lambda(\omega_f, y_F)}\left\{\frac{y_h(\omega_f)}{c_h} + 1\right. \\ &\left. - \frac{2\left[\beta_h c_h y_h(\omega_f)\right]^2}{\lambda^2(\omega_f, y_F)}\right\} I_1\left[\lambda(\omega_f, y_F)\right],\end{aligned} \tag{22}$$

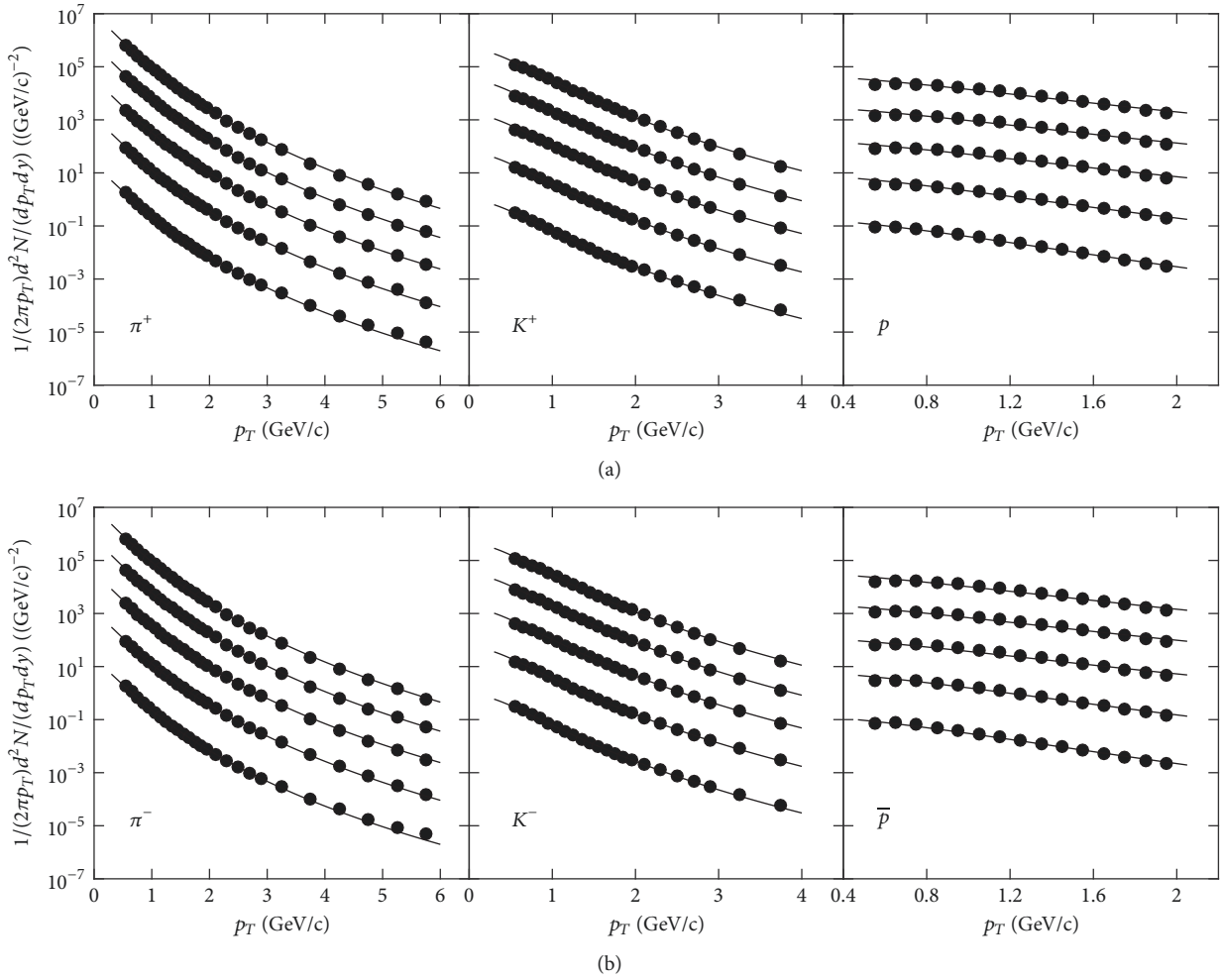

FIGURE 1: The invariant yields of $\pi^{\pm}$, $K^{\pm}$, and $p(\overline{p})$ as a function of p_T in Au+Au collisions at $\sqrt{s_{NN}} = 200$ GeV. The solid dots represent the experimental data of the PHENIX Collaboration [3]. The solid curves are the results calculated from (20). The centrality cuts counted from top to bottom in each panel are 0–10% ($\times 10^4$), 10–20% ($\times 10^3$), 20–40% ($\times 10^2$), 40–60% ($\times 10^1$), and 60–92% ($\times 10^0$), respectively.

where $\lambda(\omega_f, y_F) = \beta_h c_h \sqrt{y_h^2(\omega_f) - y_F^2}$ and I_1 is the 1st-order modified Bessel function.

By using (17) and (20)–(22), we can obtain the transverse momentum distributions of identified charged particles as shown in Figures 1 and 2.

Figure 1 shows the invariant yields of $\pi^{\pm}$, $K^{\pm}$, and $p(\overline{p})$ as a function of p_T in Au+Au collisions at $\sqrt{s_{NN}} = 200$ GeV. Figure 2 shows the same distributions in Pb+Pb collisions at $\sqrt{s_{NN}} = 2.76$ TeV. The solid dots represent the experimental data [3, 4]. The solid curves are the results calculated from (20). It can be seen that the theoretical results are in good agreement with the experimental data for $\pi^{\pm}$ and $K^{\pm}$ in the whole measured p_T region. For $p(\overline{p})$, the theoretical model works well in the region of $p_T \leq 2.0$ GeV/c. Beyond this region, the deviation appears as shown in Figure 3, which presents the fittings for $p(\overline{p})$ in the most peripheral collisions for p_T up to about 4 GeV/c.

In analyses, the sound speed in hadronic state takes the value of $c_h = 0.35$ [46–49]. The critical temperature takes the value of $T_c = 0.16$ GeV [50]. The kinetic freeze-out temperature T_f takes the values of 0.12 GeV for pions and kaons and 0.13 GeV for protons, respectively, from the investigations of [8], which also shows that the average value of baryochemical potential μ_B is about 0.019 GeV in Au+Au collisions. For Pb+Pb collisions, μ_B takes the value of $\mu_B = 0$ [8]. The initial temperature in central Au+Au and Pb+Pb collisions takes the values of $T_0 = 0.35$ GeV and $T_0 = 0.6$ GeV, respectively [51].

Tables 1 and 2 list the values of T_0, q, Q_0, and χ^2/NDF in different centrality cuts. It can be seen that T_0 decreases with increasing centrality cuts. The value of q, affecting the slopes of curves, is slightly larger than 1 for different kinds of charged particles. It is almost irrelevant to centrality cuts, while it increases with increasing beam energies and the masses of charged particles.

The parameter Q_0 has the same effects as T_0 on curves. They all affect the heights of the curves. The fitted Q_0 in Tables 1 and 2 gives the ratios

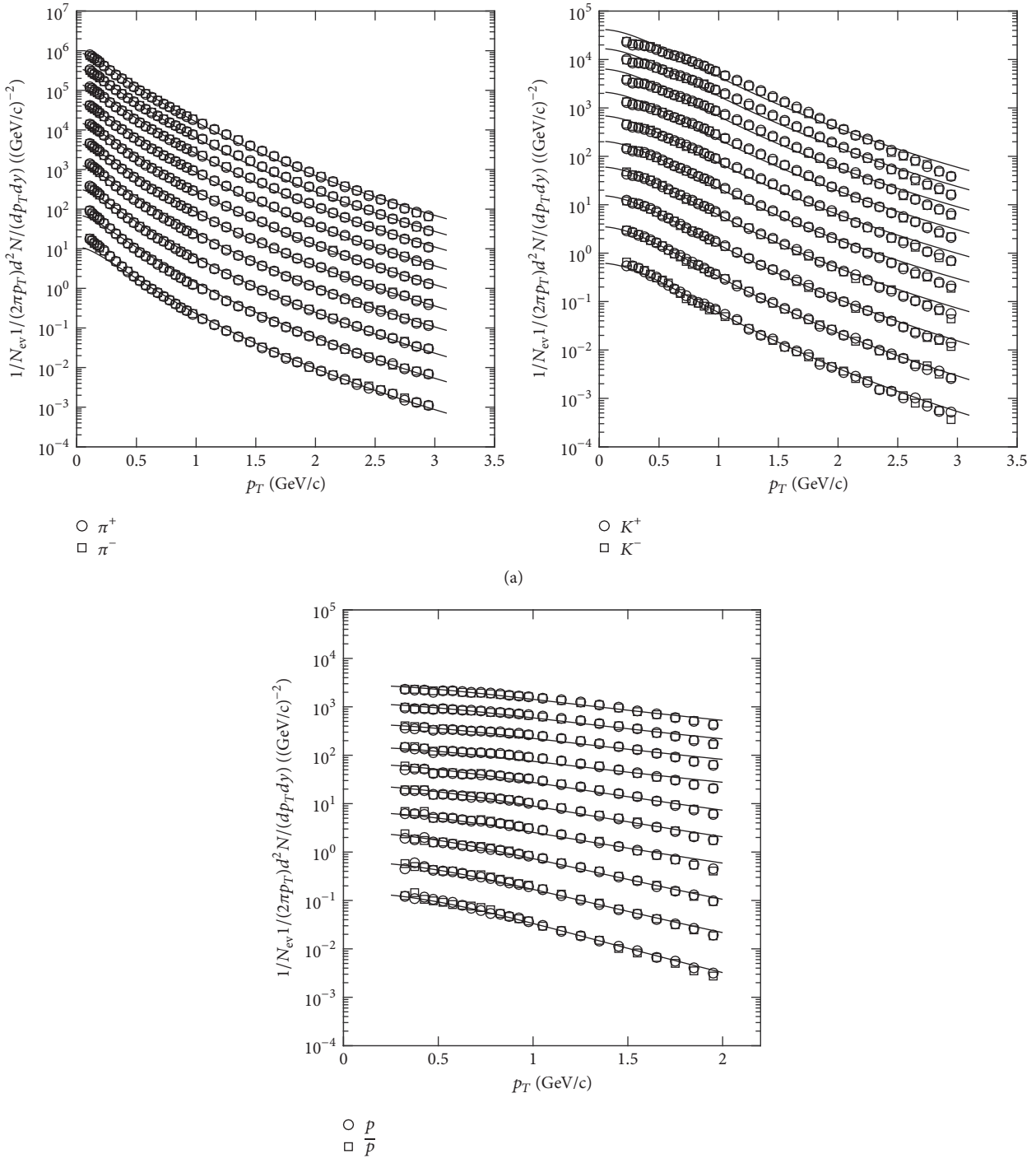

FIGURE 2: The invariant yields of $\pi^{\pm}$, $K^{\pm}$, and $p(\overline{p})$ as a function of p_T in Pb+Pb collisions at $\sqrt{s_{NN}} = 2.76$ TeV. The circles and squares represent the experimental data of the ALICE Collaboration [4]. The solid curves are the results calculated from (20). The centrality cuts counted from top to bottom in each panel are 0–5% ($\times 2^9$), 5–10% ($\times 2^8$), 10–20% ($\times 2^7$), 20–30% ($\times 2^6$), 30–40% ($\times 2^5$), 40–50% ($\times 2^4$), 50–60% ($\times 2^3$), 60–70% ($\times 2^2$), 70–80% ($\times 2^1$), and 80–90% ($\times 2^0$), respectively.

Table 1: The values of T_0, q, and Q_0 in different centrality Au+Au collisions at $\sqrt{s_{NN}} = 200$ GeV.

Centrality cuts	T_0 (GeV)	$q(\pi/K/p)$	$Q_0(\pi^+/\pi^-)$	$Q_0(K^+/K^-)$	$Q_0(p/\overline{p})$	χ^2/NDF
0–10%	0.350 ± 0.001	1.0808 ± 0.00001	0.7953 ± 0.0081	0.3552 ± 0.0043	0.4490 ± 0.0050	25/23
	0.350 ± 0.001	1.0880 ± 0.00004	0.7952 ± 0.0078	0.3315 ± 0.0040	0.3228 ± 0.0040	27/33
	0.350 ± 0.001	1.1012 ± 0.0004				18/14
10–20%	0.349 ± 0.002	1.0822 ± 0.0002	0.7953 ± 0.0112	0.3545 ± 0.0043	0.4494 ± 0.0052	20/17
	0.349 ± 0.001	1.0892 ± 0.0002	0.7965 ± 0.0110	0.3307 ± 0.0041	0.3259 ± 0.0040	21/21
	0.349 ± 0.001	1.1012 ± 0.0004				17/13
20–40%	0.320 ± 0.001	1.0838 ± 0.0002	0.7953 ± 0.0098	0.3514 ± 0.0030	0.4470 ± 0.0036	24/17
	0.320 ± 0.001	1.0904 ± 0.0003	0.8010 ± 0.0060	0.3276 ± 0.0030	0.3274 ± 0.0029	21/18
	0.320 ± 0.001	1.1012 ± 0.0002				31/32
40–60%	0.278 ± 0.001	1.0838 ± 0.0005	0.7953 ± 0.0067	0.3260 ± 0.0031	0.5494 ± 0.0048	19/14
	0.278 ± 0.001	1.0905 ± 0.0005	0.7985 ± 0.0062	0.3053 ± 0.0031	0.4093 ± 0.0038	22/10
	0.278 ± 0.001	1.0912 ± 0.0002				19/27
60–92%	0.210 ± 0.001	1.0854 ± 0.0002	0.7953 ± 0.0100	0.3134 ± 0.0033	0.9299 ± 0.0090	26/32
	0.210 ± 0.001	1.0908 ± 0.0005	0.8040 ± 0.0067	0.2943 ± 0.0032	0.7029 ± 0.0066	28/25
	0.210 ± 0.001	1.0744 ± 0.0002				3.6/9.2

Table 2: The values of T_0, q, and Q_0 in different centrality Pb+Pb collisions at $\sqrt{s_{NN}} = 2.76$ TeV.

Centrality cuts	T_0 (GeV)	$q(\pi/K/p)$	$Q_0(\pi^+/\pi^-)$	$Q_0(K^+/K^-)$	$Q_0(p/\overline{p})$	χ^2/NDF
0–5%	0.60 ± 0.02	1.104 ± 0.001	0.20 ± 0.02	0.050 ± 0.003	0.0069 ± 0.0005	1.88/2.00
	0.60 ± 0.01	1.130 ± 0.003				6.50/5.42
	0.60 ± 0.01	1.260 ± 0.005				2.35/1.50
5–10%	0.59 ± 0.02	1.104 ± 0.001	0.20 ± 0.03	0.051 ± 0.004	0.0073 ± 0.0005	2.46/2.56
	0.59 ± 0.02	1.130 ± 0.005				6.15/5.22
	0.59 ± 0.01	1.260 ± 0.004				2.75/2.15
10–20%	0.58 ± 0.02	1.104 ± 0.001	0.20 ± 0.02	0.048 ± 0.003	0.0068 ± 0.0005	2.21/2.14
	0.58 ± 0.01	1.130 ± 0.004				5.65/4.85
	0.58 ± 0.01	1.260 ± 0.004				3.43/2.79
20–30%	0.54 ± 0.01	1.104 ± 0.001	0.20 ± 0.02	0.048 ± 0.004	0.0069 ± 0.0005	2.19/2.00
	0.54 ± 0.01	1.130 ± 0.004				4.55/3.46
	0.54 ± 0.01	1.260 ± 0.004				4.60/4.08
30–40%	0.50 ± 0.02	1.104 ± 0.002	0.20 ± 0.02	0.047 ± 0.004	0.0156 ± 0.0011	2.69/2.41
	0.50 ± 0.01	1.130 ± 0.003				3.29/2.54
	0.50 ± 0.01	1.200 ± 0.004				2.27/1.87
40–50%	0.45 ± 0.01	1.103 ± 0.001	0.20 ± 0.02	0.046 ± 0.004	0.0221 ± 0.0015	2.68/2.49
	0.45 ± 0.01	1.130 ± 0.003				2.35/1.91
	0.45 ± 0.01	1.180 ± 0.003				1.89/2.00
50–60%	0.40 ± 0.01	1.103 ± 0.001	0.20 ± 0.01	0.048 ± 0.004	0.0215 ± 0.0016	5.66/5.12
	0.40 ± 0.01	1.125 ± 0.003				1.31/1.22
	0.40 ± 0.01	1.180 ± 0.002				3.97/4.86
60–70%	0.34 ± 0.01	1.100 ± 0.001	0.20 ± 0.02	0.050 ± 0.005	0.0560 ± 0.0043	5.20/4.66
	0.34 ± 0.01	1.120 ± 0.003				0.58/1.05
	0.34 ± 0.01	1.130 ± 0.003				0.91/1.25
70–80%	0.28 ± 0.01	1.100 ± 0.001	0.20 ± 0.02	0.052 ± 0.005	0.0686 ± 0.0054	8.21/7.86
	0.28 ± 0.01	1.115 ± 0.004				0.22/0.27
	0.28 ± 0.01	1.120 ± 0.002				1.01/1.43
80–90%	0.21 ± 0.01	1.099 ± 0.001	0.20 ± 0.02	0.056 ± 0.006	0.1250 ± 0.0117	6.42/5.98
	0.21 ± 0.01	1.115 ± 0.002				0.86/1.19
	0.21 ± 0.01	1.100 ± 0.003				0.40/1.42

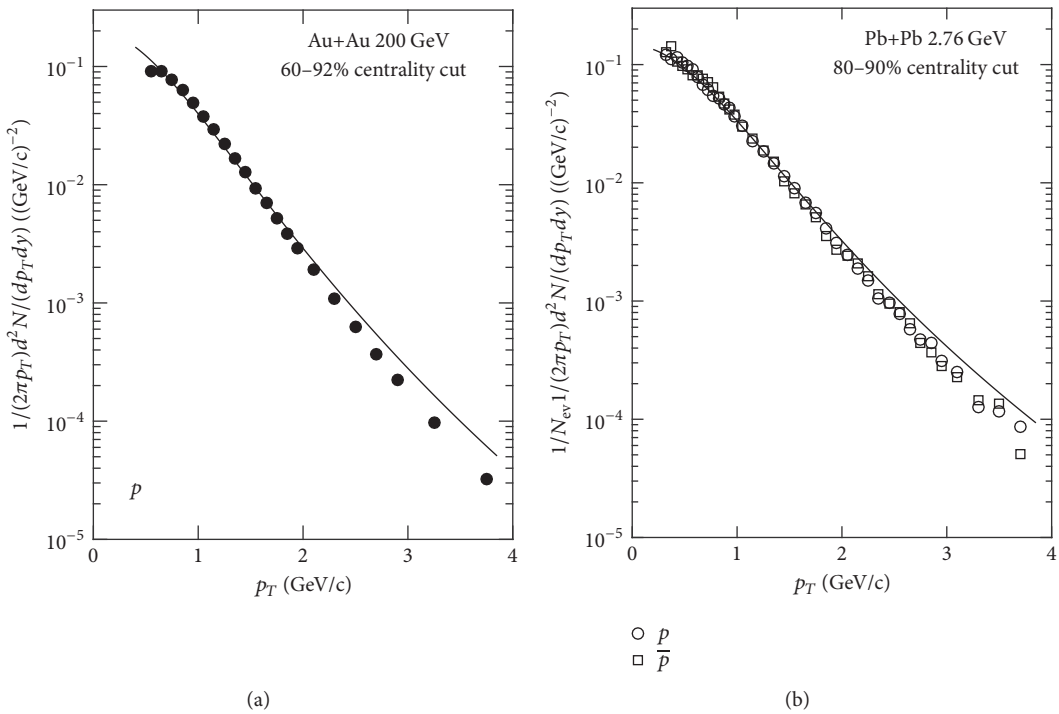

FIGURE 3: The invariant yields of $p(\overline{p})$ as a function of p_T in 60–92% Au+Au collisions at $\sqrt{s_{NN}} = 200$ GeV (a) and in 80–90% Pb+Pb collisions at $\sqrt{s_{NN}} = 2.76$ TeV (b). The meanings of solid dots, circles, squares, and solid curves are the same as those in Figures 1 and 2.

$$\frac{Q_0(\pi^-)}{Q_0(\pi^+)} = 1,$$

$$\frac{Q_0(K^-)}{Q_0(K^+)} = 0.93,$$

$$\frac{Q_0(\overline{p})}{Q_0(p)} = 0.72 \quad \text{(Au+Au 200 GeV)}, \tag{23}$$

$$\frac{Q_0(\pi^-)}{Q_0(\pi^+)} = \frac{Q_0(K^-)}{Q_0(K^+)} = \frac{Q_0(\overline{p})}{Q_0(p)} = 1 \quad \text{(Pb+Pb 2.76 TeV)}.$$

These ratios are in good agreement with the relative abundance of particles and antiparticles given in [3, 4]. This agreement may be due to the fact that the integrand of (20) is the same for particles and antiparticles in case that T_f takes a common constant for these two kinds of particles. Hence, Q_0 might be proportional to the abundance of corresponding particles.

4. Conclusions

By introducing the nonextensive statistics, we employ the relativistic hydrodynamics including phase transition to discuss the transverse momentum distributions of charged particles produced in heavy ion collisions. The model contains rich information about the transport coefficients of fluid, such as the initial temperature T_0, the critical temperature T_c, the kinetic freeze-out temperature T_f, the baryochemical potential μ_B, the sound speed in sQGP state c_0, and the sound speed in hadronic state c_h. Except for T_0, the other five parameters take the values either from widely accepted theoretical results or from experimental measurements. As for T_0, there are no widely acknowledged values so far. In this paper, T_0 takes the values referring to other studies for the most central collisions, and, for the rest of centrality cuts, T_0 is determined by tuning the theoretical results to experimental data. The present investigations show the conclusions as follows:

(1) The theoretical model can give a good description of the experimental data in Au+Au collisions at $\sqrt{s_{NN}} = 200$ GeV and in Pb+Pb collisions at $\sqrt{s_{NN}} = 2.76$ TeV for $\pi^{\pm}$ and $K^{\pm}$ in the whole measured transverse momentum region and for $p(\overline{p})$ in the region of $p_T \leq 2.0$ GeV/c.

(2) The fitted q is close to 1. This might mean that the difference between nonextensive statistics and conventional statistics is small. However, it is this small difference that plays an essential role in extending the fitting region of p_T.

(3) The fitted q increases with beam energies and the masses of charged particles. This might mean that the nonextensive statistics are more suitable for these conditions.

(4) The model cannot describe the experimental measurements for $p(\overline{p})$ in the region of $p_T \geq 2.0$ GeV/c for the both kinds of collisions. This might be caused by the hard scattering process [52]. To improve the fitting conditions, the results from perturbative QCD should be taken into account.

Conflicts of Interest

The authors declare that there are no conflicts of interest regarding the publication of this paper.

Acknowledgments

This work is supported by the Shanghai Key Lab of Modern Optical System.

References

[1] L. Adamczyk, J. K. Adkins, G. Agakishiev et al., "Centrality dependence of identified particle elliptic flow in relativistic heavy ion collisions at $\sqrt{s_{NN}}$ = 7.7–62.4 GeV," *Physical Review C*, vol. 93, Article ID 014907, 2016.

[2] J. Adam, D. Adamova, M. M. Aggarwal et al., "Anisotropic Flow of Charged Particles in Pb-Pb Collisions at $\sqrt{s_{NN}}$ = 5.02 TeV," *Physical Review Letters*, vol. 116, Article ID 132302, 2016.

[3] A. Adare, S. Afanasiev, C. Aidala et al., "Spectra and ratios of identified particles in Au+Au and d+Au collisions at $\sqrt{s_{NN}}$ = 200 GeV," *Physical Review C*, vol. 88, Article ID 024906, 2013.

[4] B. Abelev, J. Adam, D. Adamova et al., "Centrality dependence of π, K, and p production in Pb-Pb collisions at $\sqrt{s_{NN}}$ = 2.76 TeV," *Physical Review C*, vol. 88, Article ID 044910, 2013.

[5] K. Adcox, S. S. Adler, N. N. Ajitanand et al., "Single identified hadron spectra from $\sqrt{s_{NN}}$ = 130 GeV Au + Au collisions," *Physical Review C*, vol. 69, Article ID 024904, 2004.

[6] C. Adler, Z. Ahammed, C. Allgower et al., "Measurement of Inclusive Antiprotons from Au+Au Collisions at $\sqrt{s_{NN}}$ = 130 GeV," *Physical Review Letters*, vol. 87, Article ID 262302, 2001.

[7] K. Adcox, S. Belikov, J. C. Hill et al., "Centrality Dependence of $\pi\pm$, K±, p, and p Production from $\sqrt{s_{NN}}$ = 130 GeV Au+Au Collisions at RHIC," *Physical Review Letters*, vol. 88, Article ID 242301, 2002.

[8] B. I. Abelev, M. Aggarwal, Z. Ahammed et al., "Systematic measurements of identified particle spectra in pp, d+Au, and Au+Au collisions at the STAR detector," *Physical Review C*, vol. 79, Article ID 034909, 2009.

[9] B. Alver, B. Back, M. D. Baker et al., "Charged-particle multiplicity and pseudorapidity distributions measured with the PHOBOS detector in Au+Au, Cu+Cu, d+Au, and p+p collisions at ultrarelativistic energies," *Physical Review C*, vol. 83, Article ID 024913, 2011.

[10] M. Murray, "Scanning the phases of QCD with BRAHMS," *Journal of Physics G: Nuclear and Particle Physics*, vol. 30, no. 8, pp. S667–S674, 2004.

[11] M. Murray, J. Natowitz, B. S. Nielsen et al., "Flavor dynamics," *Journal of Physics G: Nuclear and Particle Physics*, vol. 35, no. 4, Article ID 044015, 2008.

[12] I. G. Bearden, D. Beavis, C. Besliu et al., "Charged Meson Rapidity Distributions in Central Au+Au Collisions at $\sqrt{s_{NN}}$ = 200 GeV," *Physical Review Letters*, vol. 94, Article ID 162301, 2005.

[13] A. Bialas, R. A. Janik, and R. Peschanski, "Unified description of Bjorken and Landau 1+1 hydrodynamics," *Physical Review C nuclear physics*, vol. 76, no. 5, Article ID 054901, 2007.

[14] C.-Y. Wong, "Landau hydrodynamics reexamined," *Physical Review C: Nuclear Physics*, vol. 78, no. 5, Article ID 054902, 2008.

[15] G. Beuf, R. Peschanski, and E. N. Saridakis, "Entropy flow of a perfect fluid in (1+1) hydrodynamics," *Physical Review C: Nuclear Physics*, vol. 78, no. 6, Article ID 064909, 2008.

[16] T. Csörgo, M. I. Nagy, and M. Csanád, "New family of simple solutions of relativistic perfect fluid hydrodynamics," *Physics Letters B*, vol. 663, no. 4, pp. 306–311, 2008.

[17] Z. W. Wang, Z. J. Jiang, and Y. S. Zhang, "The investigations of pseudorapidity distributions of final multiplicity in Au+Au collisions at high energy," *Journal of university of Shanghai for science andtechnology*, vol. 31, pp. 322–326, 2009.

[18] N. Suzuki, "One-dimensional hydrodynamical model including phase transition," *Physical Review C nuclear physics*, vol. 81, no. 4, Article ID 044911, 2010.

[19] E. K. G. Sarkisyan and A. S. Sakharov, "Relating multihadron production in hadronic and nuclear collisions," *The European Physical Journal C*, vol. 70, no. 3, pp. 533–541, 2010.

[20] A. Bialas and R. Peschanski, "Asymmetric (1+1)-dimensional hydrodynamics in high-energy collisions," *Physical Review C: Nuclear Physics*, vol. 83, no. 5, Article ID 054905, 2011.

[21] M. Csanád, M. I. Nagy, and S. Lökös, "Exact solutions of relativistic perfect fluid hydrodynamics for a QCD Equation of State," *The European Physical Journal A*, vol. 48, no. 11, pp. 173–178, 2012.

[22] Z. J. Jiang, Q. G. Li, and H. L. Zhang, "Revised Landau hydrodynamic model and the pseudorapidity distributions of charged particles produced in nucleus-nucleus collisions at maximum energy at the BNL Relativistic Heavy Ion Collider," *Physical Review C: Nuclear Physics*, vol. 87, no. 4, Article ID 044902, 2013.

[23] C. Gale, S. Jeon, and B. Schenke, "Hydrodynamic modeling of heavy-ion collisions," *International Journal of Modern Physics A*, vol. 28, no. 11, Article ID 1340011, 2013.

[24] U. Heinz and R. Snellings, "Collective flow and viscosity in relativistic heavy-ion collisions," *Annual Review of Nuclear and Particle Science*, vol. 63, pp. 123–151, 2013.

[25] A. N. Mishra, R. Sahoo, E. K. G. Sarkisyan, and A. S. Sakharov, "Effective-energy budget in multiparticle production in nuclear collisions," *The European Physical Journal C*, vol. 74, article 3147, 2014.

[26] Z. J. Jiang, Y. Zhang, H. L. Zhang, and H. P. Deng, "A description of the pseudorapidity distributions in heavy ion collisions at RHIC and LHC energies," *Nuclear Physics A*, vol. 941, pp. 188–200, 2015.

[27] H. Niemi, K. J. Eskola, and R. Paatelainen, "Event-by-event fluctuations in a perturbative QCD + saturation + hydrodynamics model: Determining QCD matter shear viscosity in ultrarelativistic heavy-ion collisions," *Physical Review C: Nuclear Physics*, vol. 93, no. 2, Article ID 024907, 2016.

[28] J. Noronha-Hostler, M. Luzum, and J.-Y. Ollitrault, "Hydrodynamic predictions for 5.02 TeV Pb-Pb collisions," *Physical Review C nuclear physics*, vol. 93, no. 3, Article ID 034912, 2016.

[29] J. S. Moreland and R. A. Soltz, "Hydrodynamic simulations of relativistic heavy-ion collisions with different lattice quantum chromodynamics calculations of the equation of state," *Physical Review C: Nuclear Physics*, vol. 93, no. 4, Article ID 044913, 2016.

[30] E. K. G. Sarkisyan, A. N. Mishra, R. Sahoo, and A. S. Sakharov, "Erratum: Multihadron production dynamics exploring the energy balance in hadronic and nuclear collisions (Physical Review D - Particles, Fields, Gravitation and Cosmology (2016) D93 (054046))," *Physical Review D: Particles, Fields, Gravitation and Cosmology*, vol. 93, no. 7, Article ID 079904, 2016.

[31] E. K. G. Sarkisyan, A. N. Mishra, R. Sahoo, and A. S. Sakharov, "Centrality dependence of midrapidity density from GeV to TeV heavy-ion collisions in the effective-energy universality picture of hadroproduction," *Physical Review D: Particles, Fields, Gravitation and Cosmology*, vol. 94, no. 1, Article ID 011501, 2016.

[32] T. Hirano, N. Van Der Kolk, and A. Bilandzic, "Hydrodynamics and flow," *Lecture Notes in Physics*, vol. 785, pp. 139–178, 2008.

[33] Z.-J. Jiang, J.-Q. Hui, and Y. Zhang, "The Rapidity Distributions and the Thermalization Induced Transverse Momentum Distributions in Au-Au Collisions at RHIC Energies," *Advances in High Energy Physics*, vol. 2017, Article ID 6896524, 8 pages, 2017.

[34] W. M. Alberico, A. Lavagno, and P. Quarati, "Nonextensive statistics, fluctuations and correlations in high energy nuclear collisions," *The European Physical Journal C*, vol. 13, pp. 499–506, 2000.

[35] M. Biyajima, T. Mizoguchi, N. Nakajima, N. Suzuki, and G. Wilk, "Modified Hagedorn formula including temperature fluctuation: Estimation of temperatures at RHIC experiments," *The European Physical Journal C*, vol. 48, no. 2, pp. 597–603, 2006.

[36] C. Tsallis, "Possible generalization of Boltzmann-Gibbs statistics," *Journal of Statistical Physics*, vol. 52, no. 1-2, pp. 479–487, 1988.

[37] T. S. Biro and G. Purcsel, "Non-extensive Boltzmann equation and hadronization," *Physical Review Letters*, vol. 95, Article ID 162302, 2005.

[38] A. S. Parvan and T. S. Biró, "Equilibrium statistical mechanics for incomplete nonextensive statistics," *Physics Letters A*, vol. 375, no. 3, pp. 372–378, 2011.

[39] T. S. Biró, G. G. Barnaföldi, and P. Ván, "Thermodynamic derivation of the tsallis and rényi entropy formulas and the temperature of quark-gluon plasma," *The European Physical Journal A*, vol. 49, no. 9, p. 110, 2013.

[40] A. R. Plastino and A. Plastino, "Information theory, approximate time dependent solutions of Boltzmann's equation and Tsallis' entropy," *Physics Letters A*, vol. 193, no. 3, pp. 251–258, 1994.

[41] D. F. Torres, H. Vucetich, and A. Plastino, "Early universe test of nonextensive statistics," *Physical Review Letters*, vol. 79, no. 9, pp. 1588–1590, 1997.

[42] G. Kaniadakis, A. Lavagno, M. Lissia, and P. Quarati, "Nonextensive statistical effects in nuclear physics problems," *Physica A: Statistical Mechanics and its Applications*, vol. 261, no. 3-4, pp. 359–373, 1998.

[43] A. K. Rajagopal, R. S. Mendes, and E. K. Lenzi, "Quantum statistical mechanics for nonextensive systems: Prediction for possible experimental tests," *Physical Review Letters*, vol. 80, no. 18, pp. 3907–3910, 1998.

[44] U. Tirnakli, F. Büyükkiliç, and D. Demirhan, "Some bounds upon the nonextensivity parameter using the approximate generalized distribution functions," *Physics Letters A*, vol. 245, no. 1-2, pp. 62–66, 1998.

[45] F. Cooper and G. Frye, "Landau's hydrodynamic model of particle production and electron-positron annihilation into hadrons," *Physical Review D: Particles, Fields, Gravitation and Cosmology*, vol. 11, pp. 192–213, 1975.

[46] T. Mizoguchi, H. Miyazawa, and M. Biyajima, "A potential including the Heaviside function in the 1 + 1 dimensional hydrodynamics by Landau : IIts basic properties and application to data at RHIC energies," *The European Physical Journal A*, vol. 40, no. 1, pp. 99–108, 2009.

[47] A. Adare, S. Afanasiev, C. Aidala et al., "Scaling properties of azimuthal anisotropy in Au+Au and Cu+Cu collisions at $\sqrt{s_{NN}}$ = 200 GeV," *Physical Review Letters*, vol. 98, Article ID 162301, 2007.

[48] L. N. Gao, Y. H. Chen, H. R. Wei, and F. H. Liu, "Speed of sound parameter from RHIC and LHC heavy-ion data," *Advances in High Energy Physics*, vol. 2013, Article ID 450247, 8 pages, 2013.

[49] S. Borsányi, G. Endrodi, Z. Fodor et al., "The QCD equation of state with dynamical quarks," *Journal of High Energy Physics*, vol. 2010, no. 11, article 77, pp. 1–31, 2010.

[50] D. Teaney, J. Lauret, and E. V. Shuryak, "A hydrodynamic description of heavy ion collisions at the SPS and RHIC," *Physical*, 2001.

[51] M. Strickland, "Thermal Y(1s) and χb1 suppression at $\sqrt{s_{NN}}$ = 2.76 TeV Pb-Pb collisions at the LHC," *Physical Review Letters*, vol. 107, no. 13, Article ID 132301, 2011.

[52] H. Lao, F. Liu, and R. A. Lacey, "Erratum to: Extracting kinetic freeze-out temperature and radial flow velocity from an improved Tsallis distribution," *The European Physical Journal A*, vol. 53, no. 6, pp. 44–64, 2017.